

Multigap superconductivity in $\text{RbCa}_2\text{Fe}_4\text{As}_4\text{F}_2$ investigated using μSR measurements

D.T Adroja,^{1,2,*} F. K. K. Kirschner,³ F. Lang,³ M. Smidman,^{4,†} A.D. Hillier,¹
Zhi-Cheng Wang,⁵ Guang-Han Cao,⁵ G. B. G. Stenning,¹ and S. J. Blundell³

¹ISIS Facility, Rutherford Appleton Laboratory, Chilton, Didcot Oxon, OX11 0QX, United Kingdom

²Highly Correlated Matter Research Group, Physics Department,

University of Johannesburg, PO Box 524, Auckland Park 2006, South Africa

³Department of Physics, University of Oxford, Clarendon Laboratory,

Parks Road, Oxford OX1 3PU, United Kingdom

⁴Center for Correlated Matter and Department of Physics, Zhejiang University, Hangzhou 310058, China

⁵Department of Physics and State Key Lab of Silicon Materials, Zhejiang University, Hangzhou 310027, China

(Dated: March 4, 2022)

The superconducting properties of the recently discovered double Fe_2As_2 layered high- T_c superconductor $\text{RbCa}_2\text{Fe}_4\text{As}_4\text{F}_2$ with $T_c \approx 30$ K have been investigated using magnetization, heat capacity, transverse-field (TF) and zero-field (ZF) muon-spin rotation/relaxation (μSR) measurements. Our low field magnetization measurements and heat capacity (C_p) reveal an onset of bulk superconductivity with $T_c \sim 30.0(4)$ K. Furthermore, the heat capacity exhibits a jump at T_c of $\Delta C_p/T_c = 94.6$ (mJ/mole-K²) and no clear effect of applied magnetic fields was observed on $C_p(T)$ up to 9 T between 2 K and 5 K. Our analysis of the TF- μSR results shows that the temperature dependence of the magnetic penetration depth is better described by a two-gap model, either isotropic $s+s$ -wave or $s+d$ -wave than a single gap isotropic s -wave or d -wave model for the superconducting gap. The presence of two superconducting gaps in $\text{RbCa}_2\text{Fe}_4\text{As}_4\text{F}_2$ suggests a multiband nature of the superconductivity, which is consistent with the multigap superconductivity observed in other Fe-based superconductors, including $\text{ACa}_2\text{Fe}_4\text{As}_4\text{F}_2$ ($A=\text{K}$ and Cs). Furthermore, from our TF- μSR study we have estimated an in-plane penetration depth $\lambda_{ab}(0) = 231.5(3)$ nm, superconducting carrier density $n_s = 7.45 \times 10^{26}$ m⁻³, and carrier's effective-mass $m^* = 2.45m_e$. Our ZF μSR measurements do not reveal a clear sign of time reversal symmetry breaking at T_c , but the temperature dependent relaxation between 150 K and 1.2 K might indicate the presence of spin-fluctuations. The results of our present study have been compared with those reported for other Fe pnictide superconductors.

PACS numbers: 74.70.Xa, 74.25.Op, 75.40.Cx

I. INTRODUCTION

The discovery of high temperature superconductivity in fluorine-doped LaFeAsO (1111-family) with a transition temperature of $T_c \sim 26$ K by Kamihara *et al.* has generated a considerable research interest world-wide to understand the nature of the superconductivity in this new class of compounds¹. It was realized soon after the discovery that the T_c of Fe-based superconductors can be increased up to 56 K as observed in $\text{Gd}_{0.8}\text{Th}_{0.2}\text{FeAsO}_2$, $\text{Sr}_{0.5}\text{Sm}_{0.5}\text{FeAsF}_3$ and $\text{Ca}_{0.4}\text{Nd}_{0.6}\text{FeAsF}_4$. Until this discovery, high temperature superconductivity in cuprates, created the impression that only Cu-O planes are pivotal for understanding the mechanism of high temperature superconductivity^{5,6}. Of course, the Fe-based superconductors do not contain Cu-O planes and some of the materials are even O free, for example, FeSe (11-family, $T_c = 8$ K at ambient pressure and 46 K in applied pressure), LiFeAs (111-family, $T_c = 18$ K), CaFeAs_2 (112-family, $T_c = 20$ K) and ThFeAsN ($T_c = 30$ K)⁷⁻¹⁰.

Another highly investigated family of Fe-based superconductors is hole (i.e. K) and electron (i.e. Co,

Ni, Rh and Pd) doped BaFe_2As_2 (122-family), which have a body centered tetragonal ThCr_2Si_2 -type structure (I4/mmm), where the ubiquitous Fe_2As_2 layers of the Fe arsenide superconductors lie between the alkaline/alkaline earth atom layers shown in Fig. 1¹¹⁻¹⁵. Recently superconductivity with $T_c \sim 35$ K has been reported in $\text{CaAFe}_4\text{As}_4$ ($A = \text{K}, \text{Rb}, \text{Cs}$, 1144-family)¹⁶ and these materials consist of different arrangements of the layers along the c-axis also displayed in Fig. 1. In this structure, the alternating arrangement of the A and Ca layers leads to two inequivalent As sites either side of the Fe sheets. The crystallographically inequivalent position of the Ca and A atoms changes the space group from I4/mmm (as for the 122-family) to P4/mmm. Further, the different valence attraction from Ca^{2+} and A^{1+} layers to $\text{Fe}_2\text{As}_2^{1.5-}$ and the different ionic radii leads to different lengths of the As-Fe bonds, which was proposed to be an important parameter for controlling the T_c of Fe-based superconductors¹⁷. Stoichiometric $\text{CaKFe}_4\text{As}_4$ is intrinsically near optimal hole doping^{16,19} and does not exhibit a high temperature structural phase transition²⁰. Similar to the optimally doped 122 compounds, probes of the gap structure and inelastic neutron scattering results strongly suggest the presence of a fully gapped s_{\pm} state^{21,22,24-26}. Further angle-resolved photoemission spectroscopy (ARPES) measurements of $\text{CaKFe}_4\text{As}_4$ re-

* devashibhai.adroja@stfc.ac.uk

† msmidman@zju.edu.cn

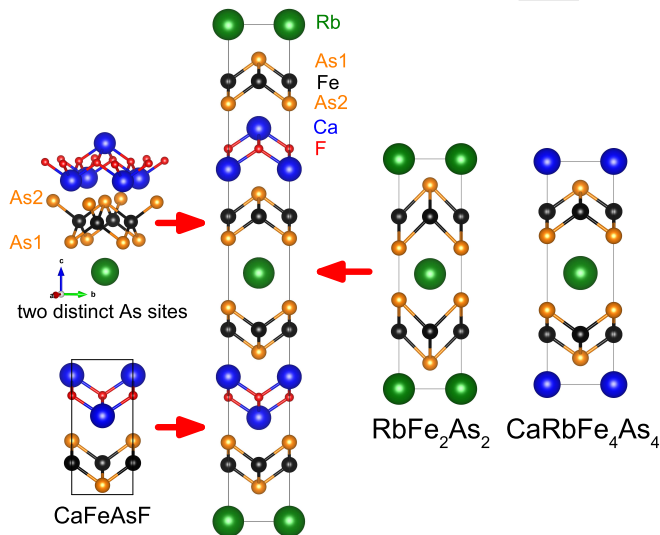


FIG. 1. (Color online) The tetragonal crystal structure of $\text{RbCa}_2\text{Fe}_4\text{As}_4\text{F}_2$. For comparison we have also given the crystal structure of RbFe_2As_2 , $\text{CaRbFe}_4\text{As}_4$ (right side) and CaFeAsF (left side bottom)^{28,29}.

port the presence of four superconducting gaps on different sheets of the Fermi surface^{21,24}, which has been explained using a four-band s_{\pm} -wave Eliashberg theory emphasizing the important role of antiferromagnetic spin fluctuations²⁷.

Very recently Zhi-Cheng Wang *et al.*^{28,29} have discovered high temperature superconductivity at 29-33 K in $\text{ACa}_2\text{Fe}_4\text{As}_4\text{F}_2$ ($A=\text{K, Rb, Cs}$, 12442-family). The crystal structure is displayed in Fig. 1, where the Fe_2As_2 layers are now sandwiched between A atoms on one side and Ca_2F_2 on the other, again leading to two distinct As sites above (As_1) and below (As_2) the Fe-plane as in 1144. These materials are also situated near to optimal doping. The electronic structure and magnetic properties of $\text{KCa}_2\text{Fe}_4\text{As}_4\text{F}_2$ have been calculated based on first-principle calculations and discussed in relation to the Fe-pnictide superconductors³⁰. There are ten bands crossing the Fermi level in the nonmagnetic (NM) state, resulting in six hole-like Fermi surface (FS) sheets along the Γ -Z line and four electron-like FS sheets along the X - P line. The shape of the FS is more complicated than other FeAs-based superconductors, showing multi-band character. Furthermore the fixed spin moment calculations and the comparisons between total energies of different magnetic phases indicate that $\text{KCa}_2\text{Fe}_4\text{As}_4\text{F}_2$ has a strong tendency towards magnetism, i.e. the stripe antiferromagnetic state. It has been found that the self-hole-doping suppresses the spin-density wave (SDW) state, inducing superconductivity in the parent compound $\text{KCa}_2\text{Fe}_4\text{As}_4\text{F}_2$ ³⁰.

The pairing symmetry of the Cooper pairs in a superconductor is manifested in an energy gap in the single-particle excitation spectrum. The superconduct-

ing gap structure is an important characteristic for a superconductor. There is experimental evidence that cuprate-based unconventional superconductors have distinct d-wave nodal gap symmetry compared with conventional phonon-mediated superconductors which have nodeless s-wave gap^{5,6}. On the other hand the superconducting gap symmetry in iron-based superconductors is rather more diverse and the subject of ongoing debate^{12,13,31,32}. Whereas nodeless gap structures have been observed in some of the doped 122-family¹¹⁻¹⁵, 1144-family^{21,22,24-26}, $\text{A}_x\text{Fe}_2\text{Se}_2$ ($A=\text{K, Cs}$)³³ and $\text{FeTe}_{1-x}\text{Se}_x$ ³⁴, the signatures of nodal superconducting gaps have been reported in LaOFeP ³⁵, LiFeP ³⁶, KFe_2As_2 ^{37,38}, $\text{BaFe}_2(\text{As}_{1-x}\text{P}_x)_2$ ³⁹, $\text{BaFe}_{2-x}\text{Ru}_x\text{As}_2$ ⁴⁰ and FeSe ⁴¹. Furthermore applied pressure and doping or chemical pressure change the gap symmetry from nodeless to nodal in $\text{Ba}_{0.65}\text{Rb}_{0.35}\text{Fe}_2\text{As}_2$ ⁴² and in $\text{BaFe}_{2-x}\text{Ni}_x\text{As}_2$ ⁴³. More interestingly the single crystal μSR study on FeSe reveals a nodeless gap (anisotropic- s -wave) along the c -axis, but one nodal and one isotropic ($s+d$ -wave) gap in the ab -plane⁴⁴.

To understand the mechanism of unconventional superconductivity and develop realistic theoretical models of Fe-based superconductors it is very important to study the pairing symmetry and the nature of the superconducting gap. There is no general consensus on the nature of pairing in iron-based superconductors leading to a variety of possibilities ranging from s_{++} wave to s_{\pm} , to d wave. Furthermore it is also important to investigate whether time-reversal symmetry (TRS) in the superconducting state is preserved or not as well as the role of spin-fluctuations. Broken symmetry can modify the physics of a system and nature of the pairing, thereby resulting in novel and uncommon behavior. Muon-spin rotation and relaxation (μSR) is an ideal and sensitive microscopic technique to investigate the properties of the superconducting state. Transverse field (TF) μSR provides information on the field distribution in the superconducting state and hence information on the penetration depth and gap symmetry. On the other hand zero-field (ZF) μSR allows the detection of very small internal fields and hence can provide direct information about whether TRS is preserved. Recently we have investigated the nature of the superconducting gap and TRS in $\text{ACa}_2\text{Fe}_4\text{As}_4\text{F}_2$ ($A=\text{K}$ and Cs) compounds using μSR measurements^{45,46}. We found two superconducting gaps with at least one nodal gap in these compounds, but no clear sign of TRS breaking. It is therefore important to investigate the gap symmetry and TRS in $A=\text{Rb}$ compound. Here we report TF- and ZF- μSR measurements of the $A=\text{Rb}$ compound. Our study shows that the superfluid density derived from the depolarization rate of the TF- μSR fits better to two isotropic gaps following a $s+s$ -wave model and ZF- μSR does not reveal any clear sign of TRS breaking below T_c .

II. EXPERIMENTAL DETAILS

The sample was characterized using powder x-ray diffraction (XRD), magnetic susceptibility and heat capacity measurements. The heat capacity was measured using a Quantum Design Physical Property Measurement System (PPMS) between 1.8 and 80 K. A standard thermal relaxation method was used with a sample mass of 8 mg. The DC magnetization measurements were carried out using a Quantum Design Magnetic Property Measurement System (MPMS). Muon spin relaxation/rotation (μ SR) experiments were carried out on the MuSR spectrometer at the ISIS pulsed muon source of the Rutherford Appleton Laboratory, UK⁴⁷. The μ SR measurements were performed in transverse-field (TF), zero-field (ZF) and longitudinal field modes. A powder sample of $\text{RbCa}_2\text{Fe}_4\text{As}_4\text{F}_2$ was mounted on a silver (99.999%) sample holder. The sample was cooled under He-exchange gas in a He-4 cryostat operating in the temperature range of 1.5 K–300 K. TF- μ SR experiments were performed in the superconducting mixed state in an applied field of $\mu_0 H_{c1} \sim 20$ mT (see Fig.2c) of this material. Data were collected in the field-cooled (FC) mode, where the magnetic field was applied above the superconducting transition temperature and the sample was then cooled down to base temperature. Muon spin rotation and relaxation is a dynamic method that allows one to study the nature of the pairing symmetry in superconductors^{48,49}. The vortex state in the case of type-II superconductors gives rise to a spatial distribution of local magnetic fields; which demonstrates itself in the μ SR signal through a relaxation of the muon polarization. Zero-field (ZF) μ SR measurements were performed from 1.2 K to 150 K in the longitudinal geometry. We also performed longitudinal field μ SR measurements at 1.2 K and 35 K. The μ SR data were analyzed using WIMDA⁵⁰.

III. RESULTS AND DISCUSSIONS

The analysis of the powder x-ray diffraction at 300 K reveals that the sample is single phase and crystallizes in the tetragonal crystal structure with space group $I4/mmm$ (No. 139, $Z = 2$) as shown in Fig. 1^{28,29}. The refined values of the lattice parameters are $a = 3.8716(1)$ Å and $c = 31.667(1)$ Å.

The low-field magnetic susceptibility measured in an applied field of 1 mT shows an onset of diamagnetism below 30 K indicating that superconductivity occurs at 30 K and the superconducting volume fraction is close to 100% at 10 K [Fig. 2(a)]. This result confirms the bulk nature of superconductivity with $T_c = 30$ K in $\text{RbCa}_2\text{Fe}_4\text{As}_4\text{F}_2$, which is comparable to $T_c = 33.3$ K and 29 K observed in $\text{ACa}_2\text{Fe}_4\text{As}_4\text{F}_2$ ($A=\text{K}$ and Cs), respectively^{28,29}.

The magnetization isotherm $M(H)$ curve at 3 K [Fig. 2(b)] shows typical behaviour for type-II superconduc-

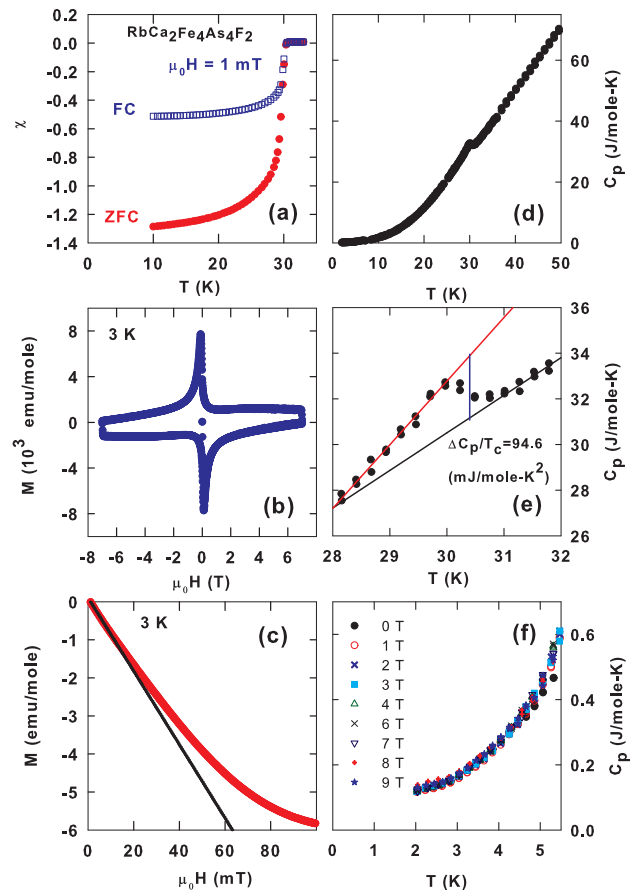


FIG. 2. (Color online) (a) Low-field dc-magnetic susceptibility measured in zero-field cooled (ZFC) and field cooled (FC) modes in an applied field of 1 mT. (b) The isothermal field dependence of magnetization at 3 K. (c) The isothermal field dependence of the magnetization at low fields at 3 K. The solid line shows a linear fit to the low field data. (d) Temperature dependence of heat capacity (C_p) versus temperature in zero field. (e) C_p vs T in an expanded scale near T_c . The solid lines show the linear fit above and below T_c and the vertical line shows the jump in the heat capacity at T_c . (f) (C_p) versus temperature in various applied magnetic fields up to 9 T.

tivity. The lower critical field H_{c1} obtained from the M vs H plot at 3 K by linear fitting the data between 0 and 15 mT is about 20 mT [Fig. 2(c)]. The upper critical field ($\mu_0 H_{c2}$) measurements using the field dependent resistivity reveals the slope $d\mu_0 H_{c2}/dT \sim -13.9$ T/K at T_c ²⁹ and the Pauli limit is $\mu_0 H_P = 1.84T_c = 55.2$ T⁵¹. Further using the orbital limiting upper critical field, $\mu_0 H_{c2}(0) = 0.73(dH_{c2}/dT)_{T_c} T_c$, we have estimated $\mu_0 H_{c2}(0) = 0.30$ kT. This value of H_{c2} gives the coherence length $\xi = (\Phi_0 / (2\pi H_{c2}))^{1/2} = 1.04$ nm, where $\Phi_0 = 2.07 \times 10^{-15}$ Tm² is the magnetic flux quantum. The specific heat (C_p) is displayed in Fig. 2(d) for zero field and an applied fields up to 9 T (Fig.2(f)). A clear anomaly is observed in the zero field C_p corresponding to the superconducting transition at around 30.4(4) K. The jump

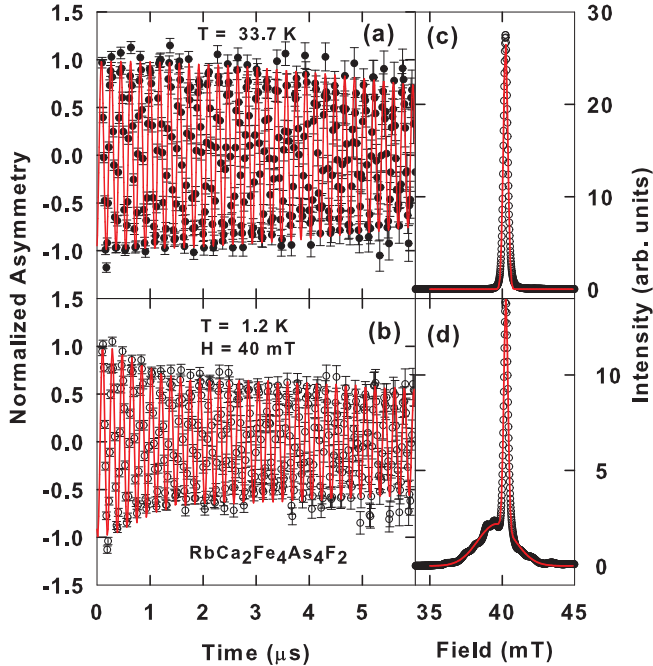


FIG. 3. (Color online) Muon spin rotation (μ SR) measurements of $\text{RbCa}_2\text{Fe}_4\text{As}_4\text{F}_2$ in a transverse field of 40 mT at (a) 33.7 K (above T_c) and (b) 1.2 K (below T_c). The solid line shows a fit using Eq.(1). (c) and (d) display the corresponding maximum entropy spectra (above and below T_c) and the red lines show fits using one (c) and two (d) Gaussian functions.

in C_p was estimated by linearly extrapolating the data above and below T_c , yielding a jump of $\Delta C_p/T_c = 94.6$ (mJ/mol K²), which is smaller than 150 (mJ/mol K²) observed in $\text{KCa}_2\text{Fe}_4\text{As}_4\text{F}_2$ ²⁸. To shed light on the nature of the gap symmetry we also performed field dependent heat capacity measurements up to a field of 9 T. We found that the heat capacity is almost independent of applied field between 2 K and 5 K.

Figures 3 (a) and (b) show the TF- μ SR precession signals above and below T_c obtained in FC mode with an applied field of 40 mT (well above $H_{c1} \sim 20$ mT but below $H_{c2} \gg 7$ T, at 3 K, see Fig.2b) and Figs. 3 (c) and (d) show the corresponding maximum entropy plots, respectively. It is clear that above T_c the μ SR spectra show a very small relaxation mainly from the quasi-static nuclear moments, and the internal field distribution is very sharp and centered near the applied field. However at 1.2 K μ SR spectra show strong damping and the internal field distribution has two components, one very sharp near the applied field and one very broad which is shifted lower than applied field. The observed decay of the μ SR signal with time below T_c is due to the inhomogeneous field distribution of the flux-line lattice. We attribute the narrow component at the applied field to muons stopping in the silver sample holder, which indicates that the field distribution within the vortex lattice is described well by

one Gaussian centered at a field below 40 mT. We have used an oscillatory decaying Gaussian function to fit the TF- μ SR time dependent asymmetry spectra:

$$A(t) = A_1 e^{-\sigma^2 t^2/2} \cos(\gamma_\mu B_1 t + \phi) + A_2 \cos(\gamma_\mu B_2 t + \phi), \quad (1)$$

where $\gamma_\mu/2\pi = 135.5$ MHz/T is the muon gyromagnetic ratio, σ is the Gaussian relaxation rate, ϕ is the phase, which is related to the detector geometry, A_1 and A_2 are the magnitudes of the terms from the sample and silver holder respectively, while B_1 and B_2 are respective internal fields. We grouped all detectors in 8 groups and all the groups were fitted simultaneously using the WIMDA software. The total amplitudes for each group of detectors were fixed. Furthermore, we first estimated the value of $A_1 \approx 0.7$ and $A_2 \approx 0.3$ by fitting the 1.2 K data and kept them fixed during the analysis allowing us to extract the temperature dependence of the relaxation rate $\sigma(T)$. Equation 1 contains the total relaxation rate σ from the superconducting fraction of the sample; there are contributions from the vortex lattice (σ_{sc}) and nuclear dipole moments (σ_{nm}) (see Fig.4b inset), where the latter is assumed to be constant over the entire temperature range [where $\sigma = \sqrt{(\sigma_{sc}^2 + \sigma_{nm}^2)}$]. The contribution from the vortex lattice, σ_{sc} , was determined by quadratically subtracting the background nuclear dipolar relaxation rate ($\sigma_{nm} = 0.138(5) \mu\text{s}^{-1}$) obtained from the spectra measured above T_c . As the applied field (40 mT) is much less than the upper critical field ($\mu_0 H_{c2} > 7$ T), σ_{sc} can be directly related to the effective penetration depth λ_{eff} using the following equation⁵²:

$$\sigma_{sc}/\gamma_\mu = 0.0609 \Phi_0 / \lambda_{\text{eff}}^2, \quad (2)$$

where Φ_0 is the magnetic flux quantum. This relation between σ_{sc} and λ_{eff} is valid for $0.13/\kappa^2 \ll (H/H_{c2}) \ll 1$, where $\kappa = \lambda/\xi \gg 70$ ⁵². Since $\text{RbCa}_2\text{Fe}_4\text{As}_4\text{F}_2$ has a two-dimensional layered crystal structure with large separation between Fe_2As_2 -layers, the out of plane penetration depth (λ_c) is much larger than that in the plane (λ_{ab}), so that the effective penetration depth can be estimated as $\lambda_{\text{eff}} = 3^{1/4} \lambda_{ab}$ ⁵³.

Furthermore the penetration depth is directly related to the normalized superfluid density, n_{ns} . In our analysis we modelled the temperature dependent normalized superfluid density using the following equation⁵⁴

$$n_{\text{ns}}(T) = \frac{\lambda_{\text{ab}}^{-2}(T, \Delta)}{\lambda_{\text{ab}}^{-2}(0)} = 1 + \frac{1}{\pi} \int_0^{2\pi} \int_{\Delta(T, \varphi)}^{\infty} \frac{\partial f}{\partial E} \frac{E dE d\varphi}{\sqrt{E^2 - \Delta^2(T, \varphi)}}, \quad (3)$$

where $f = [1 + \exp(-E/k_B T)]^{-1}$ is the Fermi function. The temperature and angular dependence of the gap is given by $\Delta(T, \varphi) = \Delta_0 \delta(T/T_c) g(\varphi)$, whereas $g(\varphi)$ refers to the angular dependence of the superconducting gap function and φ is the azimuthal angle along the Fermi

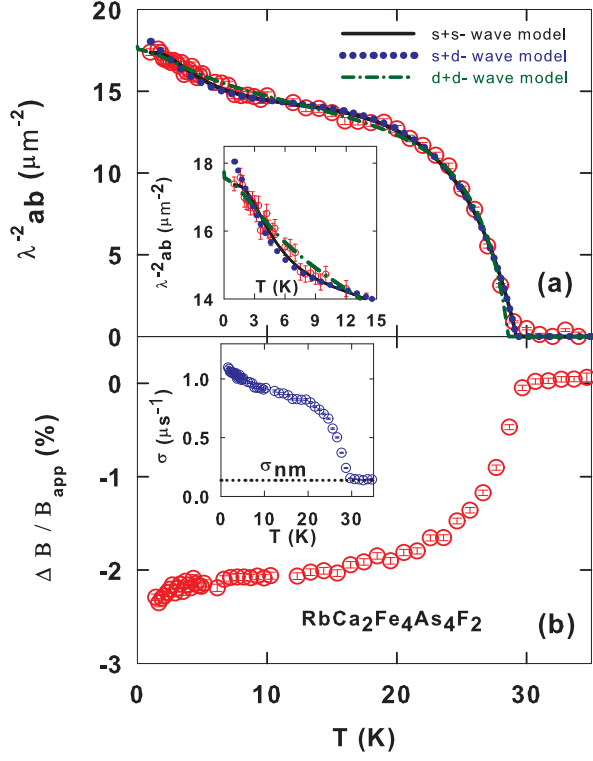


FIG. 4. (Color online) (a) Temperature dependence of λ_{ab}^{-2} of $\text{RbCa}_2\text{Fe}_4\text{As}_4\text{F}_2$. λ_{ab}^{-2} of FC mode (symbols), where the lines are the fits to the data using Eq. 3 for various two-gap models. The solid black line shows the fit using an isotropic $s+s$ -wave model with $\Delta_1(0) = 8.15 \pm 0.01$ meV and $\Delta_2(0) = 0.88 \pm 0.01$ meV, the dotted blue line shows the fit to an $s+d$ -wave model with $\Delta_1(0) = 8.08 \pm 0.02$ meV and $\Delta_2(0) = 0.92 \pm 0.01$ meV and the dashed-dotted green line shows the fit to a $d+d$ -wave model with $\Delta_1(0) = 14.05 \pm 0.26$ meV and $\Delta_2(0) = 1.26 \pm 0.02$ meV. The inset shows low temperature data in an expanded scale. (b) The normalized internal field shift as a function of temperature. The inset shows temperature dependence of total relaxation rate σ and the dotted line shows the temperature independent contribution of nuclear depolarization rate σ_{nm} .

surface. We have used the BCS formula for the temperature dependence of the gap, which is given by $\delta(T/T_c) = \tanh[(1.82)(1.018(T_c/T - 1))^{0.51}]^{55}$. $g(\varphi)^{56,57}$ is given by (a) 1 for s -wave gap [also for $s+s$ wave gap], (b) $|\cos(2\varphi)|$ for an d -wave gap with line nodes^{54,55,58}. For the two-gap analysis, we have used a weighted sum of the two components of the resulting normalized superfluid density:

$$n_{ns} = wn_{ns}(\Delta_1, T) + (1 - w)n_{ns}(\Delta_2, T) \quad (4)$$

Figure 4 (a) shows the temperature dependence of λ_{ab}^{-2} , measured in an applied field of 40 mT. λ_{ab}^{-2} increases with decreasing temperature confirming the presence of a flux-line lattice and indicates a decrease of the magnetic penetration depth with decreasing temperature. Further below 10 K λ_{ab}^{-2} shows an upturn indicating multigap behavior. The onset of diamagnetism below the superconducting transition can be seen through the decrease

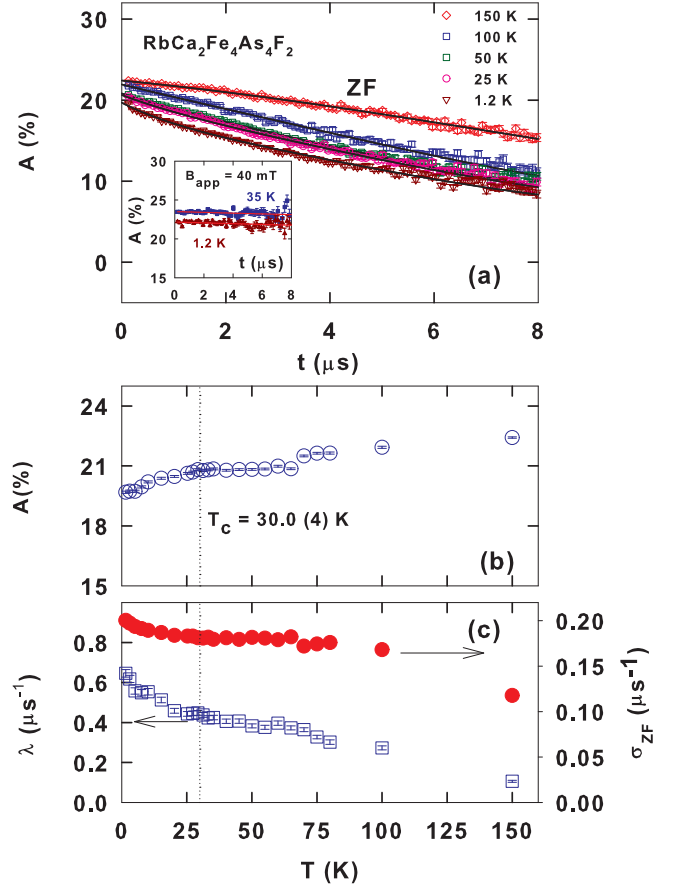


FIG. 5. (Color online) (a) Zero-field μSR spectra at four selected temperatures. The solid red lines show the fit described in the text. (b)-(c) The fit parameters versus temperature of zero-field μSR spectra of $\text{RbCa}_2\text{Fe}_4\text{As}_4\text{F}_2$. The dotted vertical line shows the transition temperature. The inset in (a) shows the spectra measured in an applied longitudinal field of 40 mT.

in the internal field below T_c as shown in Fig. 4(b). From the analysis of the observed temperature dependence of λ_{ab}^{-2} , using different models for the gap, the nature of the superconducting gap can be probed. We have analyzed the temperature dependence of λ_{ab}^{-2} based on five different models, the single gap isotropic s -wave and line nodal d -wave models, as well as isotropic $s+s$ -wave, $s+d$ -wave and $d+d$ -wave two-gap models. It was clear from the analysis that single-gap models did not fit the data (fits are not shown). The fits to the λ_{ab}^{-2} data with various two-gap models using Eq. (3) are shown by lines in Fig. 4(a) and the estimated fit parameters are given in Table. I. It is clear from the goodness of fitted χ^2 values given in Table. I that the $d+d$ -wave model does not fit the data very well. On the other hand the isotropic $s+s$ -wave, $s+d$ -wave models show good fits to the λ_{ab}^{-2} data. The value of $\chi^2 = 3.0$ for $s+s$ -wave model is slightly less than 3.1 for $s+d$ -wave model. The estimated parameters for the $s+s$ ($s+d$)-wave model show one larger gap $\Delta_1(0) = 8.15$ (8.08) (meV) and another much smaller gap $\Delta_2(0) = 0.88$ (0.92) (meV). The smaller gap is a nodal gap in the $s+d$ -wave model. Our μSR analysis suggests that an

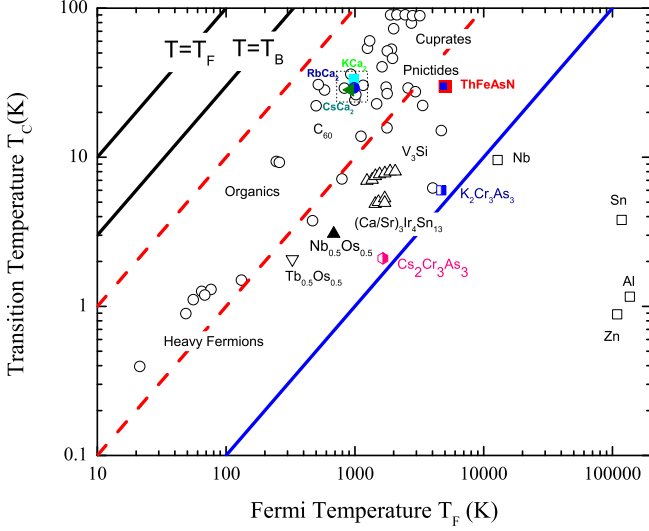


FIG. 6. (Color online) A schematic representation of the Uemura plot of superconducting transition temperature T_c against effective Fermi temperature T_F . The dotted squares shows the region where $ACa_4Fe_2As_4F_2$ ($A=K, Rb$ and Cs) compounds are located. The solid cyan square, solid blue circle and dark green horizontal triangle show the points for $A=K, Rb$ and Cs , respectively. The “exotic” superconductors fall within a common band for which $1/100 < T_c/T_F < 1/10$, indicated by the region between two red color dashed lines in the figure. The solid black line correspond to the Bose-Einstein condensation temperature (T_B).⁷⁹ The positions of $A=K, Rb$ and Cs on the plot indicate that these materials belong to exotic superconductors family.

$s+s$ -wave model explains better the temperature dependence of the superfluid density than an $s+d$ -wave model.

The value of $\lambda_{ab}(0) = 231.5 \pm 3$ nm and $T_c = 29.19 \pm 0.04$ K were estimated from the $s+s$ -wave fit. The estimated value of $2\Delta_1(0)/k_B T_c = 6.48$ from the $s+s$ -wave fit is larger than the value 3.53 expected for BCS superconductors⁵⁹, indicating the presence of strong coupling and unconventional superconductivity in $RbCa_2Fe_4As_4F_2$. On the other hand for the smaller gap the value $2\Delta_1(0)/k_B T_c = 0.7$ is much smaller than the BCS value. The two-gap nature, one larger and another smaller than the BCS value, are commonly observed in Fe-based superconductors^{60,61} as well as in $Bi_4O_4S_3$ ⁶². The observation of two isotropic gaps and nodeless superconductivity in $RbCa_2Fe_4As_4F_2$ is very similar to that observed in $CaKFe_4As_4$, where clear evidence is found for multigap nodeless superconductivity with an s_{\pm} pairing state^{21,22,24–26}. Recently we have observed two gaps in $ACa_2Fe_4As_4F_2$ ($A=K$ and Cs)^{45,46} and $ThFeAsN$ ⁶³, but at least one gap appears to be nodal in these compounds. Two superconducting gaps (one larger and another smaller) were also observed in $SrFe_{1.85}Co_{0.15}As_2$, with $T_c = 19.2$ K in an STM study⁶⁴. Moreover combined ARPES and μ SR studies on $Ba_{1-x}K_xFe_2As_2$ with $T_c = 32.0$ K also revealed the presence of two gaps ($\Delta_1 = 9.1$ meV and $\Delta_2 = 1.5$ meV)⁶⁵. The recent μ SR study on FeSe single crystals revealed that the superconducting

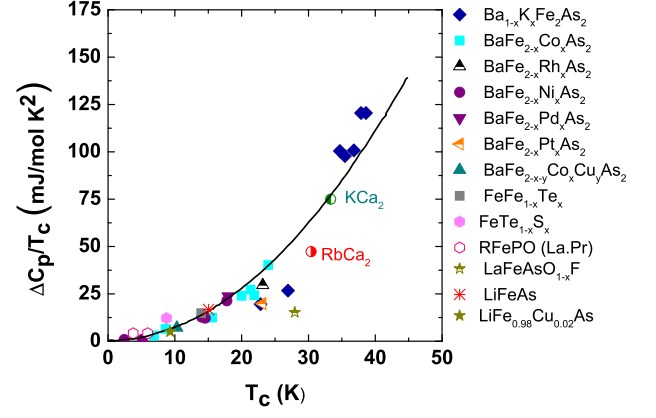


FIG. 7. (Color online) $\Delta C_p/T_c$ vs T_c for the 122-family of FeAs-based superconductors from Ref. ^{13,80}. The half filled circles red and blue colors (normalized by a factor 2 for comparison between 1244-family (4 Fe-atoms per formula unit) and 122-family (2 Fe-atoms per formula unit) are for $ACa_2Fe_4As_4F_2$ ($A=K$ and Rb) compounds, respectively. The solid line is the fit to a quadratic power law ¹³.

gap is most probably anisotropic s -wave (nodeless) along the crystallographic c -axis, but it fits better to a two-gap $s+d$ -wave model with one nodal gap in the ab -plane⁴⁴. Furthermore, nodal superconductivity has been observed in cuprate superconductors^{66,67} and the recently discovered quasi-1D Cr-based superconductors, $A_2Cr_3As_3$ ($A = K$ and Cs)^{68,69}.

As with other phenomenological parameters characterizing a superconducting state, the penetration depth can also be related to microscopic quantities. Within London theory⁴⁸, $\lambda_L^2 = \lambda_{eff}^2 = m^*c^2/4\pi n_s e^2$, where $m^* = (1 + \lambda_{e-ph})m_e$ is the effective mass and n_s is the density of superconducting carriers. Within this simple picture λ_L is independent of magnetic field. λ_{e-ph} is the electron-phonon coupling constant, which can be estimated from Θ_D and T_c using McMillan’s relation⁷⁰

$$\lambda_{e-ph} = \frac{1.04 + \mu^* \ln(\Theta_D/1.45T_c)}{(1 - 0.62\mu^*) \ln(\Theta_D/1.45T_c) + 1.04}, \quad (5)$$

where μ^* is the repulsive screened Coulomb parameter and usually assigned as $\mu^* = 0.13$. As we do not have heat capacity above 80 K for the present Rb-sample, we first estimated the value of $\Theta_{r,mD}$ for $KCa_2Fe_4As_4F_2$ by fitting the heat capacity data between 50 K and 300 K to the Debye model²⁸, which gave $\Theta_D^K = 366$ K. Then using a scaling factor⁷¹, which incorporates the differing molecular weight and unit-cell volume, we estimated $\Theta_D^{Rb} = 351.6$ K (similar for the Cs-sample $\Theta_D^{Cs} = 344.3$ K). For $RbCa_2Fe_4As_4F_2$ we have used $T_c = 29.19$ K together with $\mu^* = 0.13$ and have estimated $\lambda_{e-ph} = 1.45$. This value of λ_{e-ph} is very similar to 1.38 for $LiFeAs$ ⁷², 1.53 for $PrFeAsO_{0.60}F_{0.12}$ ⁷³ and 1.2 for $LaO_{0.9}F_{0.1}FeAs$ ⁷⁴. On the other hand for many Fe-based superconductors (11-family and 122-family) and HTSC cuprates (YBCO-123)

smaller values of $\lambda_{e-ph}=0.02$ to 0.2 and 0.02 , respectively have been reported⁷⁵. Further assuming that roughly all the normal state carriers (n_e) contribute to the superconductivity (i.e., $n_s \approx n_e$) and using the value of $\lambda_{ab}(0) = 231.5 \pm 3$ nm, we have estimated the superconducting carrier density n_s and effective-mass enhancement m^* to be $n_s = 7.45 \times 10^{26}$ carriers/m³, and $m^* = 2.45m_e$, respectively. We also estimated these parameters for $ACa_2Fe_4As_4F_2$ (A=K and Cs) samples (see Table-II) for comparison.

Zero-field μ SR measurements were performed from 1.2 K to 150 K and the results are displayed in Fig.5(a) for four selected temperatures. The data were fitted with the sum of a Lorentzian and Gaussian relaxation function

$$A_0(t) = A(a\exp(-\Lambda t) + (1-a)\exp(-\sigma_{ZF}^2 t^2/2)) + A_{bg}, \quad (6)$$

where A_{bg} is the temperature independent background arising from muons stopping on the sample holder. The value of $A_{bg}=5.898(8)\%$ and $a=0.367$ were estimated by fitting the 150 K data and were kept fixed during the analysis. At high temperature the relaxation is dominated by Gaussian decay, while at low temperature the relaxation changes to a Lorentzian decay. Moreover, there is a gradual decrease of initial asymmetry (A) with decreasing temperature, which suggests the development of fast component, which relaxes faster than the resolution of the experiment. The asymmetry exhibits a small drop below 70 K, which could be due to a competing magnetic/structural phase or related to some unknown phase transition and needs further investigation. The temperature dependence of Λ and σ_{ZF} increases with decreasing temperature between 150 K and 75 K, followed by a weak temperature dependence between 75 K and 25 K. Below 25 K both Λ and σ_{ZF} show a moderate temperature dependence. These results suggest the presence of weak magnetic fluctuations, but neither quantity shows a detectable anomaly upon passing through T_c , indicating an absence of time reversal symmetry breaking. However, since $\Lambda(T)$ and $\sigma_{ZF}(T)$ show some temperature dependence, a weak increase of the relaxation due to time reversal symmetry breaking cannot be entirely ruled out^{69,76,77}. Furthermore we also performed longitudinal fields (LF) measurements at 1.2 K and 35 K in applied LF of 25, 40 and 50 mT and the data of 40 mT field are shown in the inset of Fig. 5a. At all applied longitudinal fields, the data showed negligible relaxation (i.e the asymmetry is almost constant with time), indicating very weak spin-fluctuations which require a very small LF field to decouple the μ SR signal.

The correlation between T_c and $\sigma_{sc}(0)$ (or $\lambda_{ab}^{-2}(0)$) observed in μ SR studies has suggested a new empirical framework for classifying superconducting materials⁷⁸. Here we explore the role of muon spin relaxation rate/penetration depth in the superconducting state for the characterisation and classification of superconducting materials as first proposed by Uemura *et al.*⁷⁸. In particular we focus upon the Uemura classification scheme

which considers the correlation between the superconducting transition temperature, T_c , and the effective Fermi temperature, T_F , determined from μ SR measurements of the penetration depth⁷⁹. Within this scheme strongly correlated ‘‘exotic’’ superconductors, i.e. high T_c cuprates, heavy fermions, Chevrel phases and the organic superconductors, form a common but distinct group characterised by a universal scaling of T_c with T_F such that $1/10 > (T_c/T_F) > 1/100$ (Fig. 6). For conventional BCS superconductors $1/1000 > (T_c/T_F)$. Considering the value of $T_c/T_F = 0.04$ for $RbCa_2Fe_4As_4F_2$ (see Fig. 6), this material can be classified as an exotic superconductor, according to Uemura’s classification⁷⁸. Furthermore we have also plotted the data of $ACa_4Fe_2As_4F_2$ (A=K and Cs) in Fig. 6, which also belong to the same class.

It has been found that the jump in the heat capacity $\Delta C_p/T_c$ at T_c is also related to T_c for electron and hole doped $BaFe_2As_2$ superconductors^{13,80}. We have plotted the heat capacity jump of $ACa_2Fe_4As_4F_2$ (A=K and Rb) on the scaling plot shown in Fig.7. It is clear that for A=K and Rb compounds the heat capacity jump also follows this trend suggesting a common relation between $\Delta C_p/T_c \sim T_c^2$, the so-called BNC scaling⁸⁰.

IV. CONCLUSIONS

In conclusion, we have presented magnetization, heat capacity and transverse field (TF) and zero-field (ZF) muon spin rotation (μ SR) measurements in the normal and the superconducting state of $RbCa_2Fe_4As_4F_2$, which has a double Fe_2As_2 layered tetragonal crystal structure. Our magnetization and heat capacity measurements confirmed the bulk superconductivity with $T_c = 30.0$ (4) K. From the TF μ SR we have determined the muon depolarization rate in the FC mode associated with the vortex-lattice. The temperature dependence of the superfluid density fits better to a two-gap model, with either an isotropic $s+s$ -wave or an $s+d$ -wave gap, than to single gap isotropic s -wave or d -wave models. The $s+s$ - and $s+d$ -wave model fits give a goodness of fit (χ^2) value of 3.0 and 3.1, respectively, suggesting that an $s+s$ -wave model is an appropriate for the gap structure of $RbCa_2Fe_4As_4F_2$. Furthermore, the value (for the larger gap) of $2\Delta_1(0)/k_B T_c = 6.48 \pm 0.08$ obtained from the $s+s$ -wave model fit is larger than 3.53, expected for BCS superconductors, indicating the presence of strong coupling superconductivity, that is supported through a larger value of λ_{e-ph} , in $RbCa_2Fe_4As_4F_2$. Moreover, two superconducting gaps have also been observed in the Fe-based families of superconductors, including in other $ACa_2Fe_4As_4F_2$ (A=K and Cs) compounds and hence our observation of two gaps is in agreement with the general trend observed in Fe-based superconductors. It is an open question why the A=Rb material is more consistent with two isotropic gaps, while A=K and Cs have at least one nodal gap despite the ionic size (lattice pa-

TABLE I. Fitted parameters obtained from the fit to the $\sigma_{sc}(T)$ data of $\text{RbCa}_2\text{Fe}_4\text{As}_4\text{F}_2$ (as shown in Fig. 4(a)) using different gap models.

Model	T_c	Gap value $\Delta_1(0), \Delta_2(0)$ (meV)	Gap ratio $2\Delta(0)/k_B T_c$	w	$\lambda_{ab}^{-2}(0)$ μm^{-2}	χ^2
	K					
$s+s$ wave	29.19(4)	8.15(1); 0.88(1)	6.48; 0.70	0.79(1)	17.37(12)	3.0
$s+d$ wave	29.19(5)	8.08(2); 0.92(1)	6.42; 0.73	0.75(2)	18.66(21)	3.1
$d+d$ wave	28.57(7)	14.05(26); 1.26(2)	11.41; 1.02	0.87(2)	17.82(27)	6.2

TABLE II. The comparison of various estimated parameters, transition temperature T_c , electron-phonon coupling constant, λ_{e-ph} , carrier effective mass, m^* , superfluid density, n_s , and Fermi temperature, T_F of $\text{RCa}_2\text{Fe}_4\text{As}_4\text{F}_2$ (A=K, Rb and Cs)

Compound	T_c (K)	λ_{e-ph}	m^* (m_e)	n_s (10^{26}m^{-3})	T_F (K)
$\text{KCa}_2\text{Fe}_4\text{As}_4\text{F}_2$	33.36	1.588	2.588	8.01	741.77
$\text{RbCa}_2\text{Fe}_4\text{As}_4\text{F}_2$	29.19	1.451	2.451	7.45	727.41
$\text{CsCa}_2\text{Fe}_4\text{As}_4\text{F}_2$	28.31	1.438	2.438	6.66	652.32

rameters and unit cell volume) increasing, while T_c decreases linearly, going down the alkali atom group from K to Cs. Further confirmation of the presence of two gaps and their symmetry in $\text{RbCa}_2\text{Fe}_4\text{As}_4\text{F}_2$ could be found from angle-resolved photoemission spectroscopy (ARPES) study and TF- μ SR study on single crystals, for H||c-axis and H||ab-plane, of $\text{RbCa}_2\text{Fe}_4\text{As}_4\text{F}_2$.

ACKNOWLEDGEMENT

This work is supported by EPSRC grant EP/N023803. F.K.K.K. thanks Lincoln College, Oxford, for a doctoral

studentship and National Key R and D Program of China (Grant No. 2017YFA0303100). DTA would like to thank the Royal Society of London for the UK-China Newton mobility funding. DTA and ADH would like to thank CMPC-STFC, grant number CMPC-09108, for financial support.

-
- ¹ Y. Kamihara, H. Hiramatsu, M. Hirano, R. Kawamura, H. Yanagi, T. Kamiya, and H. Hosono, *J. Am. Chem. Soc.* **128**, 10012 (2006).
- ² C. Wang, L. Li, S. Chi, Z. Zhu, Z. Ren, Y. Li, Y. Wang, X. Lin, Y. Luo, S. Jiang, X. Xu, G. Cao, and Z. Xu, *Europhys. Lett.* **83**, 67006 (2008).
- ³ Wu, G., Y. L. Xie, H. Chen, M. Zhong, R. H. Liu, B. C. Shi, Q. J. Li, X. F. Wang, T. Wu, Y. J. Yan, J. J. Ying, X. H. Chen, *J. Phys. Condens. Matter* **21**, 206, 142203 (2009).
- ⁴ F. Chen, Pengcheng Dai, A. C. Hamann, W. Z. Hu, H. Kageyama, G. M. Luke, J. L. Luo, B. Nachumi, N. Ni, D. Reznik, D. R. Sanchez-Candela, A. T. Savici, K. J. Sikes, N. L. Wang, C. R. Wiebe, T. J. Williams, T. Yamamoto, W. Yu, and Y. J. Uemura, *Phys. Rev. B* **80**, 024508 (2009).
- ⁵ Philip W. Anderson, *J. Phys.: Conf. Ser.*, **449**, 012001 (2013).
- ⁶ B. Keimer, S. A. Kivelson, M. R. Norman, S. Uchida, J. Zaanen, *Nature*, **518**, 179, (2015)
- ⁷ Jiangang Guo, Shifeng Jin, Gang Wang, Shunchong Wang, Kaixing Zhu, Tingting Zhou, Meng He, and Xiaolong Chen, *Phys. Rev. B* **82**, 18052 (2010).
- ⁸ X. C. Wang, Q. Q. Liu, Y. X. Lv, W. B. Gao, L. X. Yang, R. C. Yu, F. Y. Li, and C. Q. Jin, *Solid State Commun.*, **148**, 538 (2008).
- ⁹ H. Yakita, H. Ogino, T. Okada, A. Yamamoto, K. Kishio, T. Tohei, Y. Ikuhara, Y. Gotoh, H. Fujihisa, K. Kataoka, H. Eisaki, and J. Shimoyama, *J. Am. Chem. Soc.* **136**, 846 (2014); N. Katayama, K. Kudo, S. Onari, T. Mizukami, K. Sugawara, Y. Sugiyama, Y. Kitahama, K. Iba, K. Fujimura, N. Nishimoto, M. Nohara, and H. Sawa, *J. Phys. Soc. Jpn.* **82**, 123702 (2013).
- ¹⁰ C. Wang, Z. C. Wang, Y. M. Mei, Y. K. Li, L. Li, Z. T. Tang, Y. Liu, P. Zhang, H. F. Zhai, Z. A. Xu, G. H. Cao, *J. Am. Chem. Soc.* **138**, 2170 (2016).
- ¹¹ P. Dai, *Rev. Mod. Phys.* **87**, 855 (2015)
- ¹² G. R. Stewart. *Rev. Mod. Phys.* **83** 1589 2011; G.R. Stewart, *Adv. in Phys.* **66**, 75 (2017)
- ¹³ J. Paglione and R. L. Greene, *Nature Physics*, **6645** (2010).
- ¹⁴ Xianhui Chen, Pengcheng Dai, Donglai Feng, Tao Xiang and Fu-Chun Zhang, *National Science Review*, **1**, 371, 2014

- ¹⁵ Marianne Rotter, Marcus Tegel, and Dirk Johrendt, *Phys. Rev. Lett.*, **101**, 107006 (2008)
- ¹⁶ A. Iyo, K. Kawashima, T. Kinjo, T. Nishio, S. Ishida, H. Fujihisa, Y. Gotoh, K. Kihou, H. Eisaki, and Y. Yoshida, *J. Am. Chem. Soc.* **138**, 3410 (2016).
- ¹⁷ Y. Mizuguchi, Y. Hara, K. Deguchi, S. Tsuda, T. Yamaguchi, K. Takeda, H. Kotegawa, H. Tou, and Y. Takano, *Supercond. Sci. Tech.* **23**, 054013 (2010).
- ¹⁸ Akira Iyo, Kenji Kawashima, Tatsuya Kinjo, Taichiro Nishio, Shigeyuki Ishida, Hiroshi Fujihisa, Yoshito Gotoh, Kunihiro Kihou, Hiroshi Eisaki, and Yoshiyuki Yoshida, *J. Am. Chem. Soc.* **138**, 3410 (2016).
- ¹⁹ W. R. Meier, T. Kong, U. S. Kaluarachchi, V. Taufour, N. H. Jo, G. Drachuck, A. E. Bohmer, S. M. Saunders, A. Sapkota, A. Kreyssig, M. A. Tanatar, R. Prozorov, A. I. Goldman, Fedor F. Balakirev, Alex Gurevich, S. L. Bud'ko, and P. C. Canfield, *Phys. Rev. B* **94**, 064501 (2016).
- ²⁰ W. R. Meier, T. Kong, U. S. Kaluarachchi, V. Taufour, N. H. Jo, G. Drachuck, A. E. Bohmer, S. M. Saunders, A. Sapkota, A. Kreyssig, M. A. Tanatar, R. Prozorov, A. I. Goldman, Fedor F. Balakirev, Alex Gurevich, S. L. Budko, and P. C. Canfield, *Phys. Rev. B* **94**, 064501 (2016).
- ²¹ Kyuil Cho, A. Fente, S. Teknowijoyo, M. A. Tanatar, K. R. Joshi, N. M. Nusran, T. Kong, W. R. Meier, U. Kaluarachchi, I. Guillamon, H. Suderow, S. L. Bud'ko, P. C. Canfield, and R. Prozorov *Phys. Rev. B* **95**, 100502 (2017).
- ²² P. K. Biswas, A. Iyo, Y. Yoshida, H. Eisaki, K. Kawashima, and A. D. Hillier, *Phys. Rev. B* **95**, 140505 (2017).
- ²³ J. Cui, Q.-P. Ding, W. R. Meier, A. E. Blohmer, T. Kong, V. Borisov, Y. Lee, S. L. Bud'ko, R. Valent, P. C. Canfield, and Y. Furukawa, *Phys. Rev. B* **96**, 104512 (2017).
- ²⁴ Daixiang Mou, Tai Kong, William R. Meier, Felix Lochner, Lin-Lin Wang, Qisheng Lin, Yun Wu, S. L. Bud'ko, Ilya Eremin, D. D. Johnson, P. C. Canfield, and Adam Kaminski, *Phys. Rev. Lett.* **117**, 277001 (2016).
- ²⁵ Kazuki Iida, Motoyuki Ishikado, Yuki Nagai, Hiroyuki Yoshida, Andrew D. Christianson, Naoki Murai, Kenji Kawashima, Yoshiyuki Yoshida, Hiroshi Eisaki, and Akira Iyo, *J. Phys. Soc. Jpn.* **86**, 093703 (2017).
- ²⁶ J. Cui, Q.-P. Ding, W. R. Meier, A. E. Bohmer, T. Kong, V. Borisov, Y. Lee, S. L. Bud'ko, R. Valenti, P. C. Canfield, and Y. Furukawa *Phys. Rev. B* **96**, 104512 (2017).
- ²⁷ G.A.Ummarino, *Physica C* **529**, 50 (2016).
- ²⁸ Zhi-Cheng Wang, Chao-Yang He, Si-Qi Wu, Zhang-Tu Tang, Yi Liu, Abduweli Ablimit, Chun-Mu Feng, and Guang-Han Cao, *J. Am. Chem. Soc.* **138**, 7856 (2016).
- ²⁹ Zhicheng Wang, Chaoyang He, Zhangtu Tang, Siqi Wu, and Guanghan Cao, *Sci. China Mater.* **60**, 83, (2017).
- ³⁰ Guangtao Wang, Zhenwei Wang and Xianbiao Shi, *EPL*, **116**, 37003 (2016).
- ³¹ H. Hosono and K. Kuroki K, *Physica C* **514** 399 (2015).
- ³² Yunkyu Bang and G R Stewart, *J. Phys.: Condens. Matter* **29**, 123003 (2017).
- ³³ Y. Zhang et al, *Nature Mater.* **10**, **273** (2011).
- ³⁴ H. Miao, P. Richard, Y. Tanaka, K. Nakayama, T. Qian, K. Umezawa, T. Sato, Y.-M. Xu, Y.-B. Shi, N. Xu, X.-P. Wang, P. Zhang, H.-B. Yang, Z.-J. Xu, J. S. Wen, G.-D. Gu, X. Dai, J.-P. Hu, T. Takahashi, H. Ding, *Phys. Rev. B* **85**, 094506 (2012).
- ³⁵ J. D. Fletcher, A. Serafin, L. Malone, J. G. Analytis, J.-H. Chu, A. S. Erickson, I. R. Fisher, and A. Carrington, *Phys. Rev. Lett.* **102**, 147001 2009
- ³⁶ J. S. Kim, L. Y. Xing, X. C. Wang, C. Q. Jin, and G. R. Stewart, *Phys. Rev. B* **87**, 054504 (2013)
- ³⁷ K.Hashimoto, A. Serafin, S. Tonegawa, R. Katsumata, R. Okazaki, T. Saito, H. Fukazawa, Y. Kohori, K. Kihou, C. H. Lee, A. Iyo ,H. Eisaki, H. Ikeda, Y. Matsuda, A. Carrington, and T. Shibauchi, *Phys. Rev. B* **82**, 014526 (2010).
- ³⁸ J. K. Dong, S. Y. Zhou, T. Y. Guan, H. Zhang, Y. F. Dai, X. Qiu, X. F. Wang, Y. He, X. H. Chen, and S. Y. Li, *Phys. Rev. Lett.* **104**, 087005 (2010).
- ³⁹ Y. Zhang, Z. R. Ye, Q. Q. Ge, F. Chen, Juan Jiang, M. Xu, B. P. Xie, and D. L. Feng, *Nature Physics* **8**, 371 (2012).
- ⁴⁰ X.Qiu, S. Y. Zhou, H. Zhang, B. Y. Pan, X. C. Hong, Y. F. Dai, Man Jin Eom, Jun Sung Kim, S. Y. Li, *Phy. Rev. X* **2**, 011010 (2012)
- ⁴¹ Can-Li Song, Yi-Lin Wang, Peng Cheng, Ye-Ping Jiang, Wei Li, Tong Zhang, Zhi Li, Ke He, Lili Wang, Jin-Feng Jia and Hsiang-Hsuan Hung, Congjun Wu, Xucun Ma, Xi Chen and Qi-Kun Xue, *Science* **332**, 1410 (2011).
- ⁴² Z. Guguchia, A. Amato, J. Kang, H. Luetkens, P.K. Biswas, G. Prando, F. von Rohr, Z. Bukowski, A. Shengelaya, H. Keller, E. Morenzoni, Rafael M. Fernandes and R. Khasanov, *Nature Commu.*, **6**, 8863 (2015).
- ⁴³ M. Abdel-Hafez, Z. He, J. Zhao, X. Lu, H. Luo, P. Dai and X.-J. Chen, arXiv:1502.07130
- ⁴⁴ Pabitra K. Biswas, Qisi Wang, A. Kreisel, D. T. Adroja, Adrian D. Hillier, Jun Zhao, Rustem Khasanov, Jean-Christophe Orain, Alex Amato and Elvezio Morenzoni, unpublished (2017).
- ⁴⁵ M. Smidman, F. K. K. Kirschner, D. T. Adroja, A. D. Hillier, F. Lang, Z. C. Wang, G. H. Cao and S. J. Blundell, arXiv:1711.10139 (2017); *Phys. Rev. B* RC at press (2018).
- ⁴⁶ F. K. K. Kirschner, D.T. Adroja, Z.-Ch. Wang, F. Lang, M. Smidman, P. J. Baker, G.-H. Cao, and S. J. Blundell, arXiv:1712.04436v1 (2017); *Phys. Rev. B* RC at press (2018).
- ⁴⁷ S. L. Lee, S. H. Kilcoyne, and R. Cywinski, *Muon Science: Muons in Physics, Chemistry and Materials* (SUSSP Publications and IOP Publishing, Bristol, 1999).
- ⁴⁸ J. E. Sonier, J. H. Brewer, and R. F. Kiefl, *Rev. Mod. Phys.* **72**, 769 (2000).
- ⁴⁹ See, for example, A. Amato, *Rev. Mod. Phys.* **69**, 1119 (1997).
- ⁵⁰ F. L. Pratt, *Physica B* **289-290**, 710 (2000).
- ⁵¹ A. M. Clogston, *Phys Rev Lett.*, **9**, 266 (1962).
- ⁵² Ernst Helmut Brandt, *Phys. Rev. B* **68**, 054506 (2003).
- ⁵³ V. I. Fesenko, V. N. Gorbunov, and V. P. Smilga, *Physica C* **176**, 551 (1991).
- ⁵⁴ R. Prozorov, and R. W. Giannetta, *Supercond. Sci. Technol.* **19**, R41 (2006).
- ⁵⁵ A. Carrington, and F. Manzano, *Physica C* **385**, 205 (2003).
- ⁵⁶ J. F. Annett, *Advances in Physics*, **39**, 83 (1990).
- ⁵⁷ G. M. Pang, M. Smidman, W. B. Jiang, J. K. Bao, Z. F. Weng, Y. F. Wang, L. Jiao, L and J. L. Zhang, and G.H. Cao, and H. Q. Yuan, *Phys. Rev. B*, **91**, 220502, (2015).
- ⁵⁸ E. E. M Chia, Elbert. S.M. Salamon, H. Sugawara and H. Sato, *Phys. Rev. B*, **69**, 180509 (R) (2004).
- ⁵⁹ J. Bardeen, L. N. Cooper, and J. R. Schrieffer, *Phys. Rev.* **106**, 162 (1957).
- ⁶⁰ D. V. Evtushinsky, D. S. Inosov, V. B. Zabolotnyy, M. S. Viazovska, R. Khasanov, A. Amato, H. -H. Klauss, H. Luetkens, Ch Niedermayer, G. L. Sun, V. Hinkov, C. T. Lin, A. Varykhalov, A. Koitzsch, M. Knupfer, B. chner, A. A. Kordyuk, and S. V. Borisenko, *New J. Phys.*, **11**, 055069 (2009).

- ⁶¹ F. Hardy, P. Burger, T. Wolf, R. A. Fisher, P. Schweiss, P. Adelman, R. Heid, R. Fromknecht, R. Eder, D. Ernst, H. v. Lohneysen, and C. Meingast, *EPL*, **91**, 47008 (2008).
- ⁶² P. K. Biswas, A. Amato, C. Baines, R. Khasanov, H. Luetkens, Hechang Lei, C. Petrovic, and E. Morenzon, *Phys. Rev. B* **58**, 224515 (2013).
- ⁶³ D. Adroja, A. Bhattacharyya, P. K. Biswas, M. Smidman, A. D. Hillier, H. Mao, H. Luo, G.-H. Cao, Z. Wang, and C. Wang, *Phys. Rev. B* **96**, 144502 (2017).
- ⁶⁴ Y. Bang and G. R. Stewart, *J. Phys: Condens. Matter*, **29**, 123003 (2017).
- ⁶⁵ R. Khasanov, D.V. Evtushinsky, A. Amato, H.-H. Klaus, H. Luetkens, Ch. Niedermayer, B. Buchner, G. L. Sun, C. T. Lin, J. T. Park, D. S. Inosov, and V. Hinkov, *Phys. Rev. Lett.* **102**, 187005 (2009).
- ⁶⁶ R. Khasanov, S. Strassle, D. Di Castro, T. Masui, S. Miyasaka, S. Tajima, A. Bussmann-Holder, and H. Keller, *Phys. Rev. Lett.* **99**, 237601 (2007).
- ⁶⁷ B. Keimer, S. A. Kivelson, M. R. Norman, S. Uchida and J. Zaanen, *Nature* **518**, 179 (2015).
- ⁶⁸ D. T. Adroja, A. Bhattacharyya, M. Smidman, A. Hillier, Y. Feng, B. Pan, J. Zhao, M.R. Lees, A. Strydom, and P.K. Biswas, *J. Phys. Soc. Jpn.*, **86**, 044710 (2017).
- ⁶⁹ D. T. Adroja, A. Bhattacharyya, M. Telling, Yu. Feng, M. Smidman, B. Pan, J. Zhao, A. D. Hillier, F. L. Pratt, and A. M. Strydom, *Phys. Rev. B* **92**, 134505 (2015).
- ⁷⁰ W. McMillan, *Phys. Rev.* **167**, 331 (1968).
- ⁷¹ V. K. Anand, D. A. Tennant and B. Lake, *J. Phys.: Condens. Matter* **27**, 436001 (2015).
- ⁷² A. A. Kordyuk, V. B. Zabolotnyy, D. V. Evtushinsky, T. K. Kim, I. V. Morozov, M. L. Kubic, R. Follath, G. Behr, B. Buchner, and S. V. Borisenko, *Phys. Rev. B* **83**, 134513 (2011).
- ⁷³ D. Bhoi, P. Mandal and P. Choudhury, *Supercond. Sci. Technol.* **21**, 125021 (2008).
- ⁷⁴ M.U. Gang, Zhu Xi-Yu, Fang Lei, Shan Lei, Ren Cong, Wend Hai-Hu, *Chin. Phys. Lett.*, **25**, 2221 (2008).
- ⁷⁵ A.-M. Zhang and Q.-M. Zhang, *Chin. Phys. B* **22**, 08710 (2013).
- ⁷⁶ R. P. Singh, A. D. Hillier, B. Mazidian, J. Quintanilla, J. F. Annett, D. M. Paul, G. Balakrishnan, and M. R. Lees, *Phys. Rev. Lett.* **112**, 107002 (2014).
- ⁷⁷ T. Shiroka, T. Shang, C. Wang, G.-H. Cao, I. Eremin, H.-R. Ott and J. Mesot, *Nature Comm.*, **8**, 156 (2017).
- ⁷⁸ Y. J. Uemura, G. M. Loke, B. J. Sternlieb, J. H. Brewer, J. F. Carolan, W. N. Hardy, R. Kadono, J. R. Kempton, R. F. Kiefl, S. R. Kreitzman, P. Mulhern, T. M. Riseman, D. Li Williams, B. X. Yang, S. Uchida, H. Takagi, J. Gopalkrishnan, A. W. Sleight, M. A. Subramanian, C. L. Chien, M. Z. Cieplak, Gang Xiao, V. Y. Lee, B. W. Statt, C. E. Stronach, W. J. Kossler and X. H. Yu, *Phys. Rev. Lett.* **62**, 2317 (1989).
- ⁷⁹ A.H. Hillier and R. Cywinski, *Appl. Mag. Reson.*, **13**, 95 (1997).
- ⁸⁰ S.L. Bud'ko, N.Ni and P. C. Canfield, *Phys. Rev. B* **79**, 220516(R) (2009).